Pergamon

Geochimica et Cosmochimica Acta, Vol. 68, No. 15, pp. 3261–3270, 2004

0016-7037/04 $30.00 + .00

doi:10.1016/j.gca.2003.12.018

Strontium incorporation into calcite generated by bacterial ureolysis

Yoshiko Fujita,[1,*] George D. Redden,[1] Jani C. Ingram,[2] Marnie M. Cortez,[1] F. Grant Ferris,[3] and Robert W. Smith[4]

[1]Idaho National Engineering and Environmental Laboratory, P.O. Box 1625, Idaho Falls, ID 83415, USA
[2]Northern Arizona University, Flagstaff, AZ 86011, USA
[3]University of Toronto, Toronto, Ontario, Canada M5S 3B1
[4]University of Idaho–Idaho Falls, Idaho Falls, ID 83402, USA

(*Received July* 1, 2003; *accepted in revised form December* 2, 2003)

Abstract—Strontium incorporation into calcite generated by bacterial ureolysis was investigated as part of an assessment of a proposed remediation approach for ^{90}Sr contamination in groundwater. Urea hydrolysis produces ammonium and carbonate and elevates pH, resulting in the promotion of calcium carbonate precipitation. Urea hydrolysis by the bacterium *Bacillus pasteurii* in a medium designed to mimic the chemistry of the Snake River Plain Aquifer in Idaho resulted in a pH rise from 7.5 to 9.1. Measured average distribution coefficients (D_{EX}) for Sr in the calcite produced by ureolysis (0.5) were up to an order of magnitude higher than values reported in the literature for natural and synthetic calcites (0.02–0.4). They were also higher than values for calcite produced abiotically by ammonium carbonate addition (0.3). The precipitation of calcite in these experiments was verified by X-ray diffraction. Time-of-flight secondary ion mass spectrometry (ToF SIMS) depth profiling (up to 350 nm) suggested that the Sr was not merely sorbed on the surface, but was present at depth within the particles. X-ray absorption near edge spectra showed that Sr was present in the calcite samples as a solid solution. The extent of Sr incorporation appeared to be driven primarily by the overall rate of calcite precipitation, where faster precipitation was associated with greater Sr uptake into the solid. The presence of bacterial surfaces as potential nucleation sites in the ammonium carbonate precipitation treatment did not enhance overall precipitation or the Sr distribution coefficient. Because bacterial ureolysis can generate high rates of calcite precipitation, the application of this approach is promising for remediation of ^{90}Sr contamination in environments where calcite is stable over the long term.

1. INTRODUCTION

The partitioning of trace elements into calcite has long been of interest for inferring the diagenetic history of authigenic carbonates. More recently, partitioning of metals in carbonates has also generated interest as a means for immobilizing toxic radionuclide or metal contaminants (e.g., ^{90}Sr, ^{60}Co, Cd) in the subsurface (e.g., Davis et al., 1987; Tesoriero and Pankow, 1996; Curti, 1999). Partitioning may occur passively, resulting in remediation analogous to "natural attenuation" as described for several organic pollutants (Wiedemeier et al., 1999), but enhancement of the process could also occur as part of an active remediation strategy. One intriguing approach is to exploit microbial activities to accelerate coprecipitation of trace metals in calcite. Carbonate mineral precipitation by microorganisms has been known for many years (Ehrlich, 1996; Castanier et al., 1999), and several different mechanisms for extracellular carbonate precipitation have been identified. Ehrlich (1996) lists five conditions that can result in solid carbonate production when appropriate cations are available, including: (1) aerobic and anaerobic oxidation of organic compounds in a well buffered neutral or alkaline environment; (2) aerobic or anaerobic oxidation of organic nitrogen compounds to produce ammonia and CO_2 in unbuffered environments; (3) reduction of gypsum to CaS by sulfate-reducing bacteria using organic electron donors; (4) the hydrolysis of urea; and (5) removal of CO_2 from bicarbonate-containing solutions.

Among the aforementioned mechanisms for microbial carbonate precipitation, the hydrolysis of urea is an especially promising approach for inducing calcite precipitation for the purpose of immobilizing contaminants in the subsurface. Urea hydrolysis results in the production of ammonium and bicarbonate, and an increase in pH (Eqn. 1). The increased alkalinity favors carbonate mineral precipitation. Eqn. 2 shows the calcite precipitation reaction at circum-neutral pH.

$$H_2NCONH_2 + 2H_2O + H + \rightarrow 2NH_4^+ + HCO_3^- \quad (1)$$

$$Ca^{2+} + 2HCO_3^- \rightarrow CaCO_3(s) + CO_2 + H_2O \quad (2)$$

In systems where CO_2 removal occurs (e.g., in a phreatic aquifer, or a vadose zone), precipitation is further enhanced. Urea hydrolyzing bacteria are widespread in the environment (Mobley and Hausinger, 1989; Fujita et al., 2000), and therefore an in situ remediation scheme based on urea hydrolysis is not likely to require the introduction of foreign microorganisms. The subsurface hydrolysis of urea offers the additional benefit of producing ammonium which can exchange for sorbed strontium and other metals (as well as calcium) on aquifer solids, resulting in their enhanced susceptibility to subsequent capture via a more permanent immobilization mechanism, in this case coprecipitation in calcite.

Ureolytically driven calcite precipitation has been previously investigated for manipulation of fluid flow in porous media (Ferris and Stehmeier, 1992; Ferris et al., 1996), for crack remediation in concrete, granite or other media (Stocks-Fischer et al., 1999; Ramachandran et al., 2001), and for calcium removal from wastewater (Hammes et al., 2003), but thus far there has been only one report on its application for contami-

* Author to whom correspondence should be addressed (fujiy@inel.gov).

nant remediation (Warren et al., 2001). Warren et al. (2001) observed that strontium uptake into calcite generated by bacterial ureolysis was significant and rapid, uranyl partitioning occurred to a lesser extent and was reversible, and copper uptake into calcite was also limited, apparently due to the toxicity of the Cu to the microorganisms (*Bacillus pasteurii*). They concluded that calcite precipitation induced by urea hydrolyzing microorganisms was a promising approach for ^{90}Sr remediation in aquifers rich in calcium carbonate.

The primary aim of the research presented here was to extend the findings of Warren et al. (2001), by examining more closely the effect of bacterial ureolysis on the uptake of strontium during calcite precipitation. Specifically, we wanted to quantify the distribution coefficient of Sr in calcite generated by bacterial ureolysis, and compare it to values reported for Sr in natural calcites or calcites generated synthetically by methods other than ureolysis. We hypothesized that the distribution coefficients for Sr in ureolytically generated calcites would be higher than in typical natural calcites, since rapid calcite precipitation can be induced by ureolysis (Stocks-Fischer et al., 1999; Fujita et al., 2000; Warren et al., 2001). Previous researchers have linked greater Sr incorporation to faster calcite precipitation (see following section), and we wanted to know whether this correlation was also applicable to ureolytically generated calcite. We also sought to characterize the mode of Sr incorporation into ureolytically generated calcite, to aid in the prediction of the long-term behavior of Sr immobilized by this mechanism.

Another motivation for this work was the need to evaluate the potential for this remediation approach in a geochemical system more closely resembling natural groundwater, unlike the artificial microbiological media used in previous studies (Fujita et al., 2000; Warren et al., 2001). In this case we were specifically interested in conditions relevant to the Snake River Plain Aquifer (SRPA), which underlies the Idaho National Engineering and Environmental Laboratory (INEEL). ^{90}Sr is a significant aquifer and vadose zone contaminant at the INEEL, as well as at a number of DOE facilities across the U.S. (Riley and Zachara, 1992). The SRPA is already supersaturated with respect to calcite (Wood and Low, 1986), and for this reason represents an ideal location for testing the application of accelerated calcite precipitation for sequestration of ^{90}Sr. Following a return to premanipulation conditions, carbonate precipitates formed in the SRPA during an engineered remediation scheme should be stable. We have previously reported the ability of groundwater microorganisms isolated from the SRPA to link urea hydrolysis and calcite precipitation in the laboratory (Fujita et al., 2000). For the experiments described here, we used Bacillus pasteurii, a well-characterized bacterium known for high urease activity and previously shown to induce calcite precipitation in urea-amended medium (Stocks-Fischer et al., 1999; Fujita et al., 2000; Warren et al., 2001). We also assessed the effect of adding bacterial cells when precipitation was driven by abiotic ammonium carbonate addition, in the absence of ureolysis. Specifically, we were interested in whether cell surfaces could themselves exert a physical control on the coprecipitation process, by aiding nucleation. We hypothesized that the addition of nucleation sites could lead to an increase in the overall nucleation rate, leading to the formation of many small crystals rather than the growth of larger crystals, as well as to more rapid precipitation. As discussed below, both factors have been implicated in increasing Sr partitioning into calcite. All experiments were conducted in synthetic groundwater designed to mimic the chemistry of the SRPA. The carbonate precipitates were analyzed for metal composition, morphology, elemental depth, and Sr bonding characteristics.

2. BACKGROUND: Sr PARTITIONING IN CALCITE

For a solid solution of Sr in calcite, at equilibrium the amount of Sr in the solid phase is related to the composition of the aqueous phase by

$$CaCO_3 + Sr^{2+} \Leftrightarrow Ca^{2+} + SrCO_3 \tag{3}$$

$$K_{EX} = \frac{K_{CaCO_3}}{K_{SrCO_3}} = \frac{\lambda_{SrCO_3} \cdot \chi_{SrCO_3} \cdot \gamma_{Ca^{2+}} \cdot m_{Ca^{2+}}}{\lambda_{CaCO_3} \cdot \chi_{CaCO_3} \cdot \gamma_{Sr^{2+}} \cdot m_{Sr^{2+}}} \tag{4}$$

$$\frac{K_{CaCO_3} \cdot \lambda_{CaCO_3} \cdot \gamma_{Sr^{2+}}}{K_{SrCO_3} \cdot \lambda_{SrCO_3} \cdot \gamma_{Ca^{2+}}} = \frac{\chi_{SrCO_3} \cdot m_{Ca^{2+}}}{\chi_{CaCO_3} \cdot m_{Sr^{2+}}} \tag{5}$$

where K_{EX} is the equilibrium constant for the exchange reaction, K_{CaCO3} and K_{SrCO3} are solubility products for pure calcite and $SrCO_3$ (with the calcite structure), respectively, γ_i and m_i are the activity coefficient and molality of the subscripted aqueous species, and χ_i and $\lambda_i$are the mole fraction and solid phase activity coefficients for the subscripted solid phases. In this case, $\chi_{SrCO3} = (1 - \chi_{CaCO3})$. In principle the equilibrium partitioning of Sr in calcite could be calculated from thermodynamic considerations. However, because of difficulties associated with determining solid phase activity coefficients and the solubility product of $SrCO_3$ in the calcite structure, an empirical distribution coefficient is generally used to describe Sr partitioning in calcite. The empirical distribution coefficient is given by an expression similar to Eqn. 5 in which the left-hand side is replaced with a constant that is dependent upon the physicochemical condition of the system:

$$D_{EX} = \frac{\chi_{SrCO_3} \cdot m_{Ca^{2+}}}{\chi_{CaCO_3} \cdot m_{Sr^{2+}}} \tag{6}$$

In batch system experiments such as those described here, the logarithmic law of Doerner and Hoskins (1925) is used to derive values of D_{EX} solely from changes in the compositions of the aqueous phase

$$\ln \frac{m_{Sr^{2+}}}{{}^{init}m_{Sr^{2+}}} = D_{EX} \ln \frac{m_{Ca^{2+}}}{{}^{init}m_{Ca^{2+}}} \tag{7}$$

where $^{init}m_i$ is the initial aqueous concentration of the subscripted species. Inspection of Eqn. 7 indicates that an average value of D_{EX} can be derived from measurements of the initial and final solution compositions. The slope of ln ($m_{Sr}^{2+}/{}^{init}m_{Sr}^{2+}$) plotted vs. ln ($m_{Ca}^{2+}/{}^{init}m_{Ca}^{2+}$) yields the value for D_{EX}.

However, previous experimental work has shown that the D_{EX} for Sr in calcite is not necessarily a constant, but is a function of precipitation rate (Lorens, 1981; Pingitore and Eastman, 1986; Tesoriero and Pankow, 1996), with higher values of D_{EX} associated with higher precipitation rates. Lorens (1981) offered an explanation related to coordination of the Sr on the calcite surface. When Sr sorbs to the growing calcite surface it is initially only partially coordinated to carbonate

oxygens, but if precipitation is slow there is time for equilibration such that only fully coordinated Sr is maintained, and the resulting distribution coefficient is close to the equilibrium value. At faster precipitation rates there is less time for equilibration, and so more Sr is trapped in the calcite lattice in partial coordination (Lorens, 1981). Pingitore and Eastman (1986) proposed another possible mechanism for the rate effect, based on the assumption that Sr can occupy both the normal lattice position of Ca and nonlattice defect sites in calcite. At higher degrees of supersaturation (e.g., faster precipitation rate), the number of crystal defects increases because surface nucleation rather than step flow is the dominant growth mechanism (Teng et al., 2000), and therefore there are more potential locations for Sr incorporation. Rimstidt et al. (1998) point out another potential contributing factor for higher Sr incorporation at faster precipitation rates. As calcite precipitation proceeds, the ratio of Sr:Ca in solution increases. At high precipitation rates, a concentration gradient develops, such that the solution boundary layer nearest the growing calcite surface has a higher Sr:Ca ratio than the bulk solution (Rimstidt et al., 1998). The higher concentration of Sr near the surface can then be trapped in the calcite, through either of the two mechanisms described above.

The observations that fast precipitation can be associated with increased Sr partitioning suggest a possible explanation for reports that microbiologically produced calcites have high (as compared to predictions based on equilibrium considerations) distribution coefficients for Sr and other trace metals (Schultzelam and Beveridge, 1994; Ferris et al., 1995). Microbial activities can alter the saturation indices for carbonate minerals, and cell surfaces can serve as nucleation sites (Ferris et al., 1987; Mcgenity and Sellwood, 1999). Both of these factors can serve to increase the rate of precipitation, and thereby increase the partitioning of Sr into calcite. Another possible factor that has been suggested is that the fine grained minerals typically formed during biomineralization (Buczynski and Chafetz, 1991) tolerate lattice substitutions more readily than larger grained minerals (Ferris et al., 1995). An objective of this research was to consider these possibilities with respect to ureolytically driven calcite precipitation.

3. MATERIALS AND METHODS

3.1. Materials

All chemicals, unless noted otherwise, were ACS reagent grade, purchased from Sigma (St. Louis, MO), Aldrich (Milwaukee, WI), Fisher (Pittsburgh, PA), J. T. Baker (Phillipsburg, NJ) or Fluka (Buchs, Switzerland).

3.2. Synthetic Groundwater

The composition of the synthetic water developed for use in the laboratory experiments was based on typical water chemistry data for the Snake River Plain Aquifer in the vicinity of the INEEL (Knobel et al., 1992). The synthetic groundwater contained KNO_3 (0.040 mM), $MgSO_4$ (0.45 mM), $CaCl_2$ (1.8 mM), $NaNO_3$ (0.040 mM), $NaHCO_3$ (1.1 mM), and $KHCO_3$ (0.062 mM). Strontium was added at 0.1 mM, as $SrNO_3$. The salts were dissolved in nanopure water (≥16+ megohms-cm; Barnstead, Dubuque, IA). For the experiments including urea, 33 mmol of reagent grade urea was added per liter of synthetic groundwater, and the medium was filter-sterilized (0.2 μm). The synthetic groundwater was prepared at 2× strength before the start of the experiments.

3.3. Coprecipitation Experiments

Bacillus pasteurii (ATCC 11859) was grown overnight in Brain Heart Infusion (BHI) broth (BD/Difco, Baltimore, MD) amended with 2% urea. *Bacillus subtilis* strain 186 (ATCC 23857) was grown overnight in tryptic soy broth (BD/Difco). Cells were harvested by centrifugation (13,000 × *g*), washed three times in sterile synthetic groundwater, and resuspended in sterile nanopure water at a fixed optical density (OD_{600} = 0.2) immediately before use in the experiments. The resulting optical density (OD_{600} = 0.1) in the reconstituted synthetic groundwater corresponded to an approximate cell density of 3.4 ± 1.2 × 10^7 cells/mL (Acridine Orange direct count; Kepner and Pratt, 1994). At the beginning of the experiments, equal volumes (200 mL) of cell suspension or sterile nanopure water (for the ammonium carbonate experiment) and sterile 2× synthetic groundwater (pH adjusted to 7.5) were mixed together, and continuous pH monitoring was initiated. The reaction vessel was maintained at 20 °C with a water bath and loosely covered, but still open to the laboratory atmosphere. The solution was continuously stirred over the course of the 8-h experiment. For the abiotic precipitation experiments, an ammonium carbonate solution was used to induce calcite precipitation. Commercial ammonium carbonate is available only as a variable mixture of ammonium carbonate and ammonium bicarbonate. Alkalinity and pH measurements suggested that our ammonium carbonate (Fisher ACS) was approximately 98.5% ammonium bicarbonate and 1.5% ammonium carbonate. A stock solution of the ammonium (bi)carbonate was added to the medium over the course of the first 15 min of the abiotic precipitation experiments to yield an estimated addition of approximately 34.6 mEq/L ammonium. At predefined intervals, sample aliquots were removed from the experimental flasks for Ca and Sr measurement (5 mL) and for urea measurement (1 mL), if applicable. All sample aliquots were immediately filtered (0.2 μm) and stored at 4 °C or frozen until analysis. At the end of the 8 h experiment, precipitates were collected by centrifugation.

Saturation indices (log Q/K where Q is the ion activity product and K is the corresponding equilibrium constant) were calculated for calcite and strontianite using The Geochemist Workbench (GWB) Software package (Release 4.0, Rockware Inc., Denver, CO; Bethke, 2002) and the supplied Lawrence Livermore National Laboratory (LLNL) thermodynamic database. The GWB package calculates activity coefficients using the B-dot extension of the Debye-Hückel method of Helgeson (1969). Initial conditions for the experiments were undersaturated (saturation index ≤0) with respect to both calcite and strontianite.

3.4. Measurement of Urea

Urea was measured by an adaptation of the spectrophotometric method reported by Knorst et al. (1997). Briefly, a filtered sample (1 mL) containing urea was reacted with 0.25 mL of an ethanolic solution of *p*-dimethylaminobenzaldehyde (4% w/v) and sulfuric acid (4% w/v). After 5 min, the colored product was measured by UV spectrophotometry (Shimadzu UV-1601, Shimadzu Corporation, Kyoto, Japan) at 422 nm. Samples were compared with external standards prepared in nanopure water; previous experience indicated that calibration curves for standards in nanopure water and in the synthetic groundwater were identical.

3.5. Measurement of Ca, Sr by ICP-AES

Ca and Sr were measured in both solid and aqueous samples by inductively coupled plasma with atomic emission spectrophotometric detection (ICP-AES). Precipitates were initially dissolved in nitric acid. Filtered aqueous samples were acidified with nitric acid (pH<2). The metal concentrations were measured on a Thermo Jarrell Ash Iris II system (Thermo Elemental, Franklin, MA, USA). The instrument was operated and calibrated in accordance with the manufacturer's instructions. A sample spike and replicate analyses were performed to assure accuracy and precision of the analysis. Calibration standards were prepared from commercial stock solutions. An internal standard of yttrium was spiked to each sample and all standards at 2 ppm to correct for any matrix problems. A continuing calibration verification standard and a continuing calibration blank were analyzed throughout the anal-

ysis to monitor instrument performance. The wavelengths used for analysis were 317.933, 346.446, and 371.030 nm for Ca, Sr, and Y, respectively.

3.6. XRD

For X-ray diffraction (XRD) analyses of the precipitates, the material was hand-ground and mounted on glass slides. The samples were analyzed with a Bruker D-8 Advance X-ray Diffractometer (Bruker AXS, Congleton, Cheshire, UK) with a Cu tube source (30 mA–40 kV), single Gobels mirror and a scintillation detector. Bruker "Eva" software was used to evaluate the samples.

3.7. ESEM and EDS

Direct examination and elemental analysis of the precipitates produced during the experiments were conducted with environmental scanning electron microscopy (ESEM) and energy dispersive X-ray spectroscopy (EDS). Images were collected with a Philips XL30 ESEM equipped with a LAB6 electron source (FEI Co., Hillsboro, OR, USA). Within the ESEM sample chamber, samples were maintained at 3 °C with a Peltier cooling stage. The wet samples were deposited onto 6 mm stainless steel coupons (polished to 6 μm) designed to fit into the metal cup supplied with the Peltier stage. The cells were not fixed. Water vapor pressure was varied from 5.9 to 4.1 torr, corresponding to relative humidity in the sample chamber of 100 to 73%, respectively. Relative humidity was varied during imaging in attempts to improve visualization of individual bacterial cells. Accelerating voltages were varied from 7 keV to 10 keV.

To image bacterial cells, *B. pasteurii* cells deposited on a stainless steel coupon were placed under vacuum in a Hummer V sputter coater (Technics, Inc., Advanced Technologies, San Diego, CA, USA) fitted with a gold target and coated with ~10 nm of gold. The sample was then imaged in high vacuum mode at 10 keV.

The ESEM was equipped with a Princeton Gamma-Tech EDS system (Princeton Gamma-Tech, Princeton, NJ, USA) capable of detecting light elements. The system allows determination of bulk elemental composition as well as estimates of relative atomic proportions within the sample utilizing standardless quantitative analysis. X-ray collection was performed at 15 keV accelerating voltage with an Ultra Thin Window to obtain total counts of 100,000 to 150,000 (2–5% dead time) with good spectral resolution.

3.8. ToF-SIMS Analysis and Determination of Sputter Depth by AFM

To characterize Sr incorporation with depth into the precipitates, time-of-flight secondary ion mass spectrometry (ToF-SIMS) analyses were performed using a Charles Evans & Associates instrument (Schueler et al., 1990), in the user facility at the Image and Chemical Analysis Laboratory at Montana State University. The solid particles were pressed into indium foil and coated with 10 nm of gold before mounting in the sample holder to prevent charging. The sample was then admitted to the analysis chamber and analyzed at a base pressure of $\sim 5 \times 10^{-9}$ torr. The primary ion was a microfocused Ga^+ gun operated at ~1 nA dc current at +15 keV energy. The sample was held at 3 keV potential; hence, the impact energy of the primary ions was 12 keV. The mass resolution ($m/\Delta m \sim 1200$) was sufficient to distinguish inorganic from organic ions. The analytical protocol consisted of collecting a positive ion mass spectrum, sputtering the sample, and then repeating the processes. The sample was sputtered for 2.5, 5.0, 7.5, 10, 12.5, 15, 20, 35, and 50 min, resulting in a total of 10 mass spectra at 10 different depths. During the depth profiling 2×10^{-6} torr oxygen was leaked into the chamber and an 80×80 μm area was sputtered employing the primary beam previously described. Care was exercised to maintain the emission current of the liquid metal ion gun during sputtering. The instrument was pumped down to $\sim 5 \times 10^{-9}$ torr before analysis, and within each sputtered zone only a 12×12 μm area was analyzed.

Atomic force microscopy (AFM; Digital Instruments Dimension 3100, Santa Barbara, CA, USA) was used to determine sputter depth for sputter depth profiling. A calcite crystal spar (Iceland Calcite 46 E 1438; Ward's Natural Science, Rochester, NY) was used for the determination due to its flatness. The sample was sputtered for 10 min. under the same conditions used for SIMS analysis, then imaged by AFM.

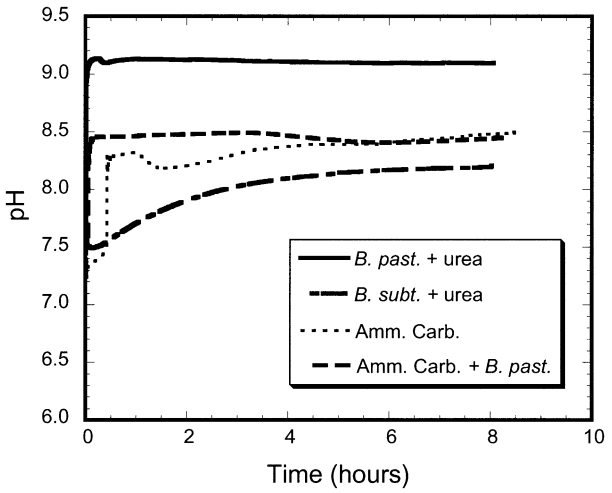

Fig. 1. pH trends in calcite precipitation experiments. Experiments conducted at 20 °C.

3.9. X-ray Absorption Near-Edge Spectroscopy (XANES)

X-ray absorption analysis was performed at Argonne National Laboratory's Advanced Photon Source on beamline 20 with bending magnet X-rays (PNC-CAT line 20-BM). A Si (111) double-crystal monochromator was used with a slit of approximately 1 mm × 10 mm at 50 m from the source, detuned by 50% to reduce harmonics. Energy resolution was 3.5–4 eV. Detectors were custom ion chambers filled with Ar/N_2 gas mixtures (approx. 1:1 for transmission, and 1:0 for fluorescence).

Powdered strontium carbonate and strontium nitrate reference solids, and test samples were mounted as approximately 1 mm layers using Kapton tape. Beam alignment was based on use of fluorescent film and maximum fluorescence/absorbance at 16,200 eV (Sr absorption edge is 16,105 eV). A zirconium metal foil was used for monochromator calibration (first absorption inflection point at 17,998 eV; Bearden and Burr, 1967). Four to five scans were collected and averaged for each sample. Pre-edge background subtraction and XANES normalization were performed by fitting linear polynomials separately to the pre-edge and post-edge regions.

4. RESULTS AND DISCUSSION

4.1. Solution Chemistry Changes

Upon introduction of the *B. pasteurii* to the synthetic groundwater containing urea, the pH rose to approximately 9.1 within the first quarter hour, and remained at that level for the duration of the experiment (Fig. 1). Urea measurements indicated that 30 mM was hydrolyzed within the first hour; urea concentrations did not change over the next 7 h of the experiment (data not shown). The change in pH was correlated with the changes in Ca and Sr; solution concentrations for both ions dropped dramatically within the first hour and remained at approximately the same concentrations for the rest of the experimental time period (Fig. 2). The saturation index for calcite at the end of the experiment was 1.1, as compared to an initial value of −0.2. The production of white solids was visually observed within the first hour. In contrast, in the experimental system with *B. subtilis* no decrease in urea concentration was detected.

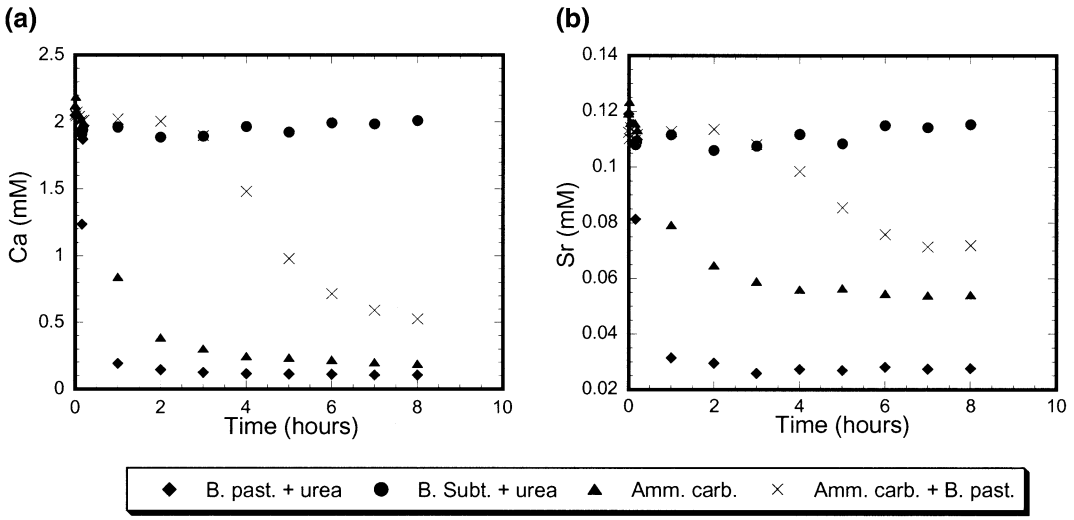

Fig. 2. Solution profiles for (a) calcium and (b) strontium during coprecipitation experiments. Experiments conducted at 20 °C.

Although physiologic information (Atkinson and Fisher, 1991) and genomic information (Cruz-Ramos et al., 1997) confirm the presence of urease and urease genes in *B. subtilis* 186, this organism did not exhibit ureolytic activity under the conditions of these experiments, and therefore was a suitable nonureolytic control. The initial drop in pH observed with the *B. subtilis* may have been attributable simply to the initial mixing of the experimental solutions; the *B. subtilis* cell suspension was at pH 6.5 before mixing with the 2× synthetic groundwater. And although a gradual increase in pH to a final value of 8.2 was observed (Fig. 1), no decreases in Ca and Sr concentrations were observed over the course of the experiment (Fig. 2), and no visible precipitates were formed after 8 h.

Because pure "ammonium carbonate" was not available, it was not possible to precisely simulate the urea hydrolysis experiment in the abiotic precipitation experiments. The amount of inorganic carbon that was added in the abiotic experiments was similar to the increase that resulted from urea hydrolysis by *B. pasteurii*. However, the increase in alkalinity (and ammonium) was only half that of the urea hydrolysis experiment. Consequently our main goal was to compare the two abiotic treatments to each other, evaluating the effect of adding non-urea hydrolyzing cell surfaces. In addition, the ammonium carbonate experiments allowed us to extend the range of precipitation rates examined for their effect on Sr partitioning (see section 4.5). In both ammonium carbonate treatments the pH eventually rose to approximately 8.5 (Fig. 1) and dissolved Ca and Sr decreased (Fig. 2). In both cases Ca and Sr removal occurred at a slower rate than with urea hydrolysis, as would be expected given that the alkalinity increase was approximately one half (i.e., HCO_3^- rather than CO_3^{2-}) of that which resulted from urea hydrolysis. However, in the presence of the *B. pasteurii* cells, the onset of Ca and Sr removal was delayed and the overall removal of the ions from solution after 8 h was reduced relative to the case without cells (Fig. 2). Final calcite saturation indices for the ammonium carbonate and ammonium carbonate + cells treatments were 1.0 and 1.4, respectively. One might have expected that the addition of bacterial cell surfaces, which are known to have high binding capacities for metals (Douglas and Beveridge, 1998) and can serve as mineral nucleation sites (Ehrlich, 1999), would enhance the precipitation rate, but we did not observe any such enhancement. Friis et al. (2003) reported that *B. subtilis* cells caused decreased calcite saturation indices due to uptake of Ca on cell wall functional groups (Friis et al., 2003). This process could explain our observations, although the cell densities that Friis et al. (2003) reported to have an effect, on the order of 10^{11} cells/mL, were more than three orders of magnitude higher than what was tested here. Organic biomolecules associated with the cells may have suppressed calcite precipitation. LeBron and Suarez (1996) reported that dissolved organic carbon at concentrations >0.05 mM inhibits calcite growth (Lebron and Suarez, 1996). In the case of urea hydrolyzing *B. pasteurii*, it is possible that the active metabolism creates such strong gradients at the cell surface that the inhibiting effects of organic moieties are overcome.

4.2. ESEM, EDS, and XRD of Precipitates

Samples of the white solids that formed in the reaction vessels were examined by ESEM. The precipitates produced during bacterial ureolysis were roughly rhombohedral in shape, and generally 5–10 μm on a side. Indentations and holes that correlated with the size and shape of the bacteria were clearly evident throughout the precipitates (Fig. 3a). The bacteria themselves were difficult to image with the sample preparation technique utilized for the ESEM of the crystals; gold coating of the bacteria and subsequent imaging (Fig. 3b) showed that the *B. pasteurii* cells were indeed of the size to match the observed holes in the precipitates. Apparently the precipitation occurred directly on and in the immediate vicinity of the cells, suggesting that the cells served as nucleation sites. In contrast, the crystals produced in the ammonium carbonate experiments without cells (Fig. 3c) showed no evidence of the holes, although the crystals were similar in overall size and shape to the ones generated by ureolysis. When the *B. pasteurii* cells were

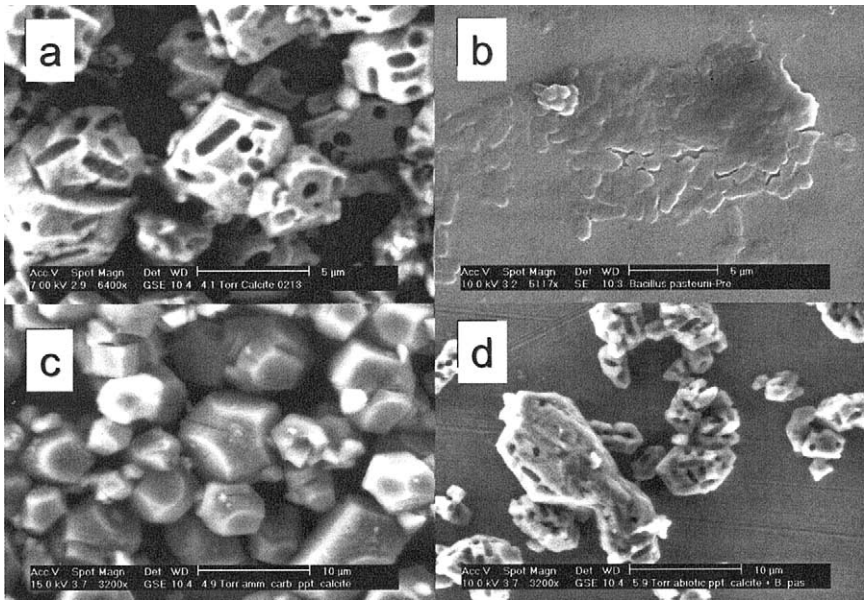

Fig. 3. Scanning electron micrographs of (a) calcite produced by *B. pasteurii* hydrolyzing urea, (b) gold coated *B. pasteurii* cells, (c) calcite produced by the addition of ammonium carbonate in the absence of cells, and (d) calcite produced by the addition of ammonium carbonate in the presence of *B. pasteurii*, but in the absence of urea.

added to the ammonium carbonate samples, in the absence of urea, similar holes were seen in the precipitates but the morphology of the precipitates was not as regular (Fig. 3d). The size range of the particles however was similar to the other precipitates, with dimensions generally on the order of 5–10 μm. EDS spectra of all three types of precipitates were similar, clearly showing a large Ca peak and a smaller Sr peak (data not shown). XRD analyses of all of the precipitates indicated only the presence of calcite in the samples, although calculated saturation indices for strontianite at the conclusion of the precipitate-producing experiments were 3.3 to 3.5.

4.3. Sr:Ca Ratios in Precipitates

Sputter depth profiling with ToF SIMS was used to determine whether the Sr concentration varied as a function of depth in the calcite crystals. The Sr:Ca ratios shown in Figure 4 were calculated from the ion intensities for *m/z* 88 (Sr) and *m/z* 40 (Ca). The ratios were corrected for the mass selectivity of the detector, but not for the natural isotopic abundances of the elements; consequently the values are true isotopic ratios, rather than elemental ratios. The elemental ratios would be higher, by a factor of 1.17. The depth into the precipitates was estimated from ToF SIMS experiments with reference calcite and AFM. In these studies, 10 min of sputtering time was correlated to a depth of 710Å. In all three treatments, Sr was present at depth within the calcite, and was not just present as a surface phase. The *B. pasteurii* and urea treatment exhibited a consistently higher Sr:Ca ratio throughout the depth investigated (up to ~350 nm) as compared to the particulates generated by ammonium carbonate addition. In particular, the Sr:Ca ratio appeared to be elevated near the surface of the particles. This result is consistent with precipitation in a batch system at low temperature, where the composition of the aqueous phase changes as precipitation proceeds (in this case, the solution becomes progressively enriched in Sr), and ionic solid state diffusion is slow, hindering reequilibration of the solid with the aqeuous phase (Prieto et al., 1997). It is likely that this effect was most pronounced in the *B. pasteurii* + urea treatment because it resulted in the most calcite precipitation, and thus the solution composition changed to the greatest extent. The inclusion of *B. pasteurii* cells in the ammonium carbonate treatment did not significantly affect the near surface Sr:Ca ratios.

Elemental Sr:Ca ratios for the bulk precipitates were measured following acidic digestion and analysis by ICP-AES (Table 1). These data also demonstrate the enhanced uptake of

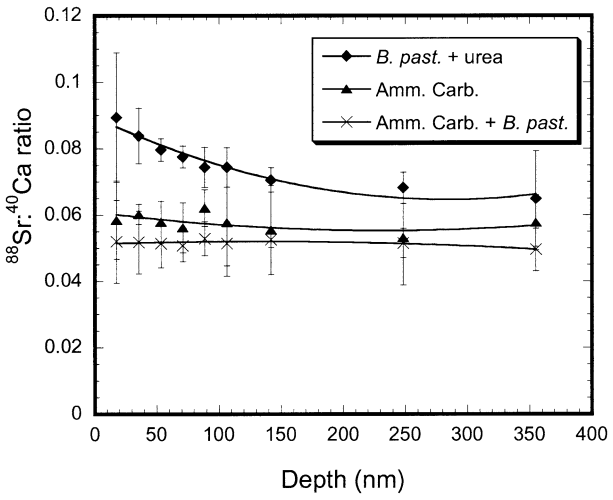

Fig. 4. Isotopic ratio of Sr:Ca with depth into the calcite precipitates, determined by ToF SIMS. Ratios were calculated from the ion intensities for *m/z* 88 (Sr) and *m/z* 40 (Ca).

Table 1. Sr:Ca ratios in precipitates measured by ICP-AES after acidic digestion.

Sample generated by:	Sr:Ca
B. pasteurii + urea	0.044
Ammonium carbonate	0.032
Ammonium carbonate + *B. pasteurii*	0.027

Sr into the precipitates generated by *B. pasteurii* and urea, relative to the ammonium carbonate generated samples. The precipitate generated by ammonium carbonate addition in the presence of *B. pasteurii* had a slightly lower Sr:Ca ratio than the ammonium carbonate treatment alone, but this lower ratio is likely due to the slower precipitation rate observed for the former system (discussed in section 4.5). For all three of the sample types, comparison with the ToF SIMS data shows that the bulk Sr:Ca ratios of the solids were considerably lower than the estimated ion ratios in the near surface, indicating that the ion ratio must have dropped significantly with increasing depth into the particles. As the particles were on the order of 5–10 μm in depth, and the ToF SIMS data were only acquired for approximately the outer 350 nm of the particles, only the outer ~5–10% of the particles were analyzed by ToF SIMS. As previously noted, this outer layer represents calcite grown during the later stages of precipitation, when the Sr:Ca ratio in solution is highest.

4.4. Sr Coordination in Calcite

Figure 5 shows X-ray absorption spectra for the experimental precipitates, along with reference spectra for $SrCO_3$ and $Sr(NO_3)_2$ solids. The primary absorption edge inflection points for $SrCO_3$ and $Sr(NO_3)_2$ were at 16,110 eV. Edge inflection points for the experimental samples were all at 16,111 eV. The reported standard value for the Sr absorption edge is 16,105 eV (Bearden and Burr, 1967). Spectra for the experimental samples were essentially identical to each other, and clearly differ-

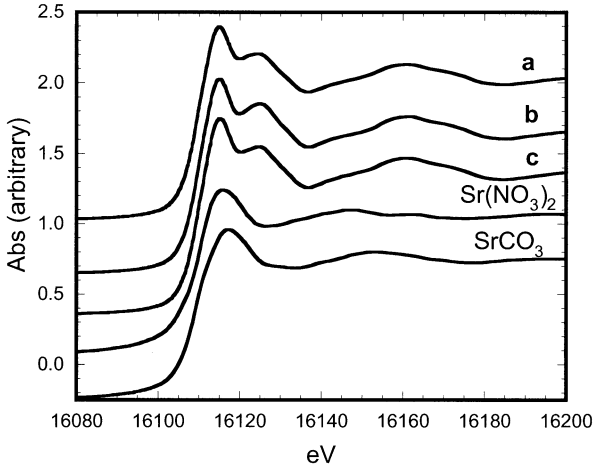

Fig. 5. Sr K-edge XANES of calcites generated in experimental treatments (a) *B. pasteurii* + urea, (b) ammonium carbonate, and (c) ammonium carbonate + *B. pasteurii*, compared to reference spectra for $SrCO_3$ and $Sr(NO_3)_2$.

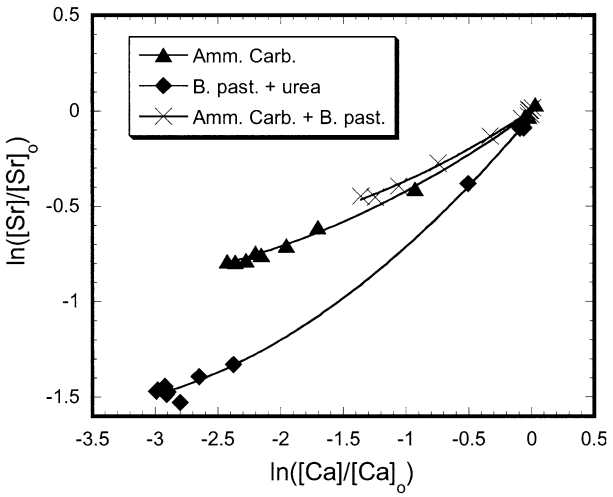

Fig. 6. Plot of ln ($m_{Sr}^{2+}/^{int}m_{Sr}^{2+}$) vs. ln ($m_{Ca}^{2+}/^{int}m_{Ca}^{2+}$) for the experimental treatments that resulted in calcite precipitation.

ent from the reference spectra for $SrCO_3$ and $Sr(NO_3)_2$. Single peaks at approximately 16,118 eV are seen in the XANES region (0–30 eV above the absorption edge) for strontianite and strontium nitrate, while the spectra for the experimental treatments all show two peaks at approximately 5 and 14 eV above the absorption edge. In addition, peaks in the EXAFS region, above approximately 16,150 eV, can be discerned in the experimental treatments, and there are no equivalent features for the strontianite sample. Solutions of Sr salts were not analyzed in this project, however a spectrum for 100 mM $SrCl_2$ was reported by Parkman et al. (1998). This spectrum also shows a single peak in the XANES region, indicating that Sr is not present as a hydrated ion in the experimental samples.

Our spectra were similar to those reported by Pingitore et al. (1992) in their study of Sr incorporation into natural and synthetic calcites. Pingitore et al. (1992) interpreted their spectra as evidence for Sr substitution at Ca structural sites. In an EXAFS analysis of calcite, strontianite, and samples of Sr coprecipitated with $CaCO_3$, Parkman et al. (1998) verified an approximately hexacoordinate structure for strontium in the calcite lattice. Overall, the most logical interpretation for the Sr coprecipitated with $CaCO_3$ in these experiments is that Sr is present predominantly as a substitution in the calcite lattice. This interpretation is consistent with the results of the ToF SIMS analyses, which showed Sr present in the interior of the calcite, rather than present only as a sorbed surface phase.

4.5. Strontium Distribution Coefficients

Plots of ln ($m_{Sr}^{2+}/^{init}m_{Sr}^{2+}$) vs. ln ($m_{Ca}^{2+}/^{init}m_{Ca}^{2+}$) for the 3 experiments in which calcite precipitation occurred are nonlinear, indicating that D_{EX} is not constant (Fig. 6). These results show that in general the *B. pasteurii* plus urea experiment was associated with greater partitioning of Sr into calcite (overall slope = 0.49, based on t=0 and t=8 concentrations) than either of the nonureolytic controls (overall slope = 0.33), and the distribution coefficient decreased over time.

One of the goals of this study was to assess whether Sr partitioning in calcite precipitated as a result of ureolytic ac-

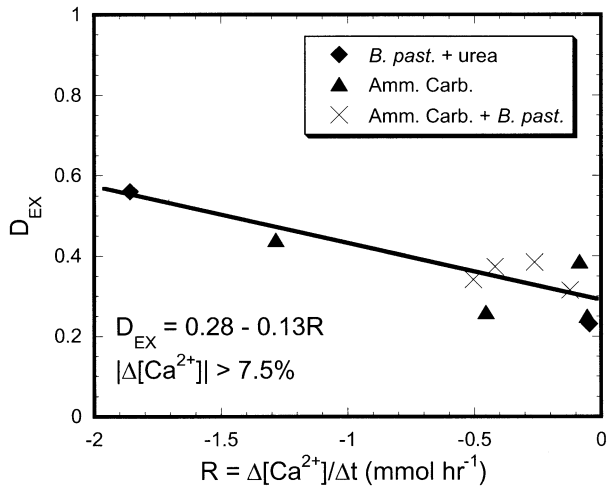

Fig. 7. Values of D_{EX} plotted as a function of the average precipitation rate for the calcite precipitation experiments. Precipitation rates were estimated by evaluating the changes in solution concentration of Sr and Ca that occurred between hourly samplings of the solution over the 8 h course of the experiments. Values of D_{EX} and precipitation rates for which there was less than 7.5% change in the concentration of calcium were excluded, because the uncertainty in our determination of individual concentrations was estimated to be 3% and differences between measurements of less than ~6% are insignificant.

tivity is fundamentally different from Sr partitioning in calcite precipitated by abiotic processes or if urea hydrolysis influences Sr^{2+} partitioning solely by its effects on the rate of calcite precipitation. As previously discussed, high rates of precipitation are known to result in greater Sr partitioning into calcite. Figure 7 shows values of D_{EX} plotted as a function of the average precipitation rate for the experiments shown in Figure 6. Precipitation rates were estimated by evaluating the changes in Ca concentration that occurred between hourly samplings of the solution phase. The results shown in Figure 7 suggest that all of the experiments can be described by a single trend and support the hypothesis that biotic urea hydrolysis influences Sr^{2+} partitioning primarily through the precipitation rate, rather than through a structural effect related to the bacterial surface or particulars of metabolism. The addition of bacterial cell surfaces to the ammonium carbonate treatment did not appear to enhance Sr uptake, through either an increased precipitation rate or some other mechanism, although the appearance of the crystals did suggest that the cells served as nucleation sites. The apparent primary dependence of Sr partitioning on the precipitation rate is in contrast to the findings of Roden et al. (2002), where Sr partitioning into biogenic siderite was greater than into abiotically generated siderite even when the respective precipitation rates were comparable. One potential explanation offered for that result was that the reduced proton activity engendered by bacterial iron reduction could have increased the tendency for Sr^{2+} to sorb to reactive sites on the siderite surfaces, thereby promoting surface enrichment and entrapment of Sr during crystal growth. It is possible that this mechanism may have also been operative during our experiments with the alkalinity-producing urea hydrolysis reaction, but its effect was overwhelmed by the high rates of precipitation generated in our experiments. In our experiments, extensive precipitation occurred over the course of a few hours; in the Roden et al. (2002) experiments, Sr uptake into solids occurred over the course of weeks.

Extrapolation of the trend shown in Figure 7 to very slow precipitation rates yields a value of D_{EX} of 0.28. This value is much higher than the values (0.02–0.1) reported in the summary of Rimstidt et al. (1998) and at the higher end of the range reported by Curti (1999). The high value (0.40) of Curti (1999) is taken from Mucci and Morse (1983) who reported results of Sr^{2+} partitioning into calcite with significant amounts of Mg and is probably not applicable to the current study. The large discrepancy between our value of D_{EX} and previous studies may be due to the mode of calcite precipitation. Previous studies have focused on the growth of calcite on preexisting calcite seed crystals. In this study the dominant mode of precipitation was nucleation in a system free of preexisting calcite. Reeder et al. (1999) found that divalent trace metal ions both smaller and larger than calcium substitute into calcium sites within the calcite structure with varying degrees of local distortion. The smaller crystal sizes associated with nucleated calcite may more readily accommodate the distortion than larger crystals and permit more extensive substitution. Lebron and Suarez (1996) suggest that for many subsurface waters the concentration of dissolved organic carbon may be high enough to effectively eliminate crystal growth as a precipitation mode, leaving nucleation as the most important precipitation mode. If nucleation is indeed the most important mode of calcite precipitation in soil and groundwater, the higher values of D_{EX} reported in the current study may not be so extreme, when considering potential distribution coefficients that could be achieved in an engineered system. Whether in fact nucleation is the dominant mode of precipitation in natural groundwater is however unclear. Tobin et al. (2000) reported Sr concentrations of 40 to 50 ppm for calcites collected from the SRPA in eastern Idaho. If these calcite compositions are representative of partitioning with current groundwater (Sr^{2+}:Ca^{2+} ratios of 0.00285, unpublished data), a much lower value (0.02) of D_{EX} is suggested. This lower value is consistent with the ranges reported by Curti (1999) and Rimstidt et al. (1998), and argues against nucleation as the dominant precipitation mode for the SRPA. However, the current groundwater may not have the same composition as that responsible for the precipitated calcite (Tobin et al., 2000).

5. CONCLUSIONS

To develop a remediation approach based on the in situ immobilization of a contaminant in a solid phase, it is necessary to maximize the sequestration of the contaminant, verify that it is stable over the long-term, and be able to control the process in time and place. The research reported here contributes to initial efforts to address the first two needs with respect to Sr coprecipitation in calcite. The results support earlier suggestions that enhanced Sr uptake is associated with carbonates generated by biotic processes (Ferris et al., 1995; Warren et al., 2001), in particular by bacterial ureolysis. Our data indicate that this enhanced uptake is primarily due to the high precipitation rates that can be generated by bacterial ureolysis. Work is currently underway in our laboratories to investigate this phenomenon more rigorously, with detailed kinetic analysis

and modeling. The effects on the strontium partitioning of any physical controls exerted by the cell surfaces appear to be negligible. The main role of the ureolytic cells appears to be in changing the solution geochemistry. XANES analyses indicate that the Sr incorporated into calcite through the activity of urea hydrolyzing organisms is present in the form of a solid solution, ensuring the relative stability of ^{90}Sr immobilized in calcite through this mechanism. As Pingitore et al. (1992) point out, "no significant alteration of the strontium in geological calcites should occur, barring the actual dissolution of the material." This robustness bodes well for the potential application of the proposed remediation approach as a long-term containment and stabilization strategy for ^{90}Sr in environments such as the SRPA where calcite is stable.

Acknowledgments—We thank B. White, C. Watkins and A. Erickson at the INEEL for assistance with the ICP-AES, ESEM/EDS and XRD analyses respectively, and R. Avci of the Image and Chemical Analysis Laboratory at Montana State University for assistance with the ToF-SIMS and AFM analyses. We are grateful to C. Palmer and also to three anonymous reviewers for their constructive comments. Funding for this work was provided by the INEEL through the U.S. Department of Energy contract DE-AC07-99ID13727, and by the U.S. DOE Environmental Management Science Program through award DE-FG07-99ER15025. Use of the Advanced Photon Source was supported by the U.S. DOE, Office of Science, Office of Basic Energy Sciences, under Contract No. W-31-109-Eng-38. Access to the beamlines managed by the Pacific Northwest Consortium Collaborative Access Team (PNC-CAT) was made available and facilitated with the expertise, advice, and generous assistance of S. Heald and R. Gordon of the Argonne National Laboratory. The beamline is supported by US DOE Office of Science grant no. DE-FG03-97ER45628.

Associate editor: P. A. Maurice

REFERENCES

Atkinson M. R. and Fisher S. H. (1991) Identification of genes and gene-products whose expression is activated during nitrogen-limited growth in *Bacillus subtilis*. *J. Bacteriol.* **173,** 23–27.

Bearden J. A. and Burr A. F. (1967) Reevaluation of X-ray atomic energy levels. *Rev. Mod. Phys.* **39,** 125–142.

Bethke C. M. (2002) The Geochemist's Workbench: A User's Guide to Rxn, Act2, Tact, React, and Gtplot (Release 4.0). University of Illinois, Urbana, IL.

Buczynski C. and Chafetz H. S. (1991) Habit of bacterially induced precipitates of calcium-carbonate and the influence of medium viscosity on mineralogy. *J. Sediment. Petrol.* **61,** 226–233.

Castanier S., Le Metayer-Levrel G., and Perthuisot J. P. (1999) Ca-carbonates precipitation and limestone genesis—The microbiogeologist point of view. *Sediment. Geol.* **126,** 1–4 9–23.

Cruz-Ramos H., Glaser P., Wray L., Jr., and Fisher S. (1997) The *Bacillus subtilis* ureABC operon. *J. Bacteriol.* **179,** 3371–3373.

Curti E. (1999) Coprecipitation of radionuclides with calcite: Estimation of partition coefficients based on a review of laboratory investigations and geochemical data. *Appl. Geochem.* **14,** 433–445.

Davis J. A., Fuller C. C., and Cook A. D. (1987) A model for trace-metal sorption processes at the calcite surface—Adsorption of Cd^{2+} and subsequent solid-solution formation. *Geochim. Cosmochim. Acta* **51,** 1477–1490.

Doerner H. A. and Hoskins W. M. (1925) Co-precipitation of radium and barium sulfates. *J. Am. Chem. Soc.* **47,** 662–675.

Douglas S. and Beveridge T. J. (1998) Mineral formation by bacteria in natural microbial communities. *FEMS Microbiol. Ecol.* **26,** 79–88.

Ehrlich H. L. (1996) *Geomicrobiology.* Marcel Dekker.

Ehrlich H. L. (1999) Microbes as geologic agents: Their role in mineral formation. *Geomicrobiol. J.* **16,** 135–153.

Ferris F. G. and Stehmeier L. G. (1992) U.S. Patent, Pat. No. 5,143,155. *Bacteriogenic Mineral Plugging.*

Ferris F. G., Fratton C. M., Gertis J. P., Schultzelam S., and Lollar B. S. (1995) Microbial precipitation of a strontium calcite phase at a groundwater discharge zone near Rock Creek, British Columbia, Canada. *Geomicrobiol. J.* **13,** 57–67.

Ferris F. G., Stehmeier L. G., Kantzas A., and Mourits F. M. (1996) Bacteriogenic mineral plugging. *J. Can. Petrol. Technol.* **35,** 56–61.

Ferris F. G., Fyfe W. S., and Beveridge T. J. (1987) Bacteria as nucleation sites for authigenic minerals in a metal-contaminated lake sediment. *Chem. Geol.* **63 (***3–4***),** 225–232.

Friis A. K., Davis T. A., Figueira M. M., Paquette J., and Mucci A. (2003) Influence of *Bacillus subtilis* cell walls and EDTA on calcite dissolution rates and crystal surface features. *Environ. Sci. Technol.* **37,** 2376–2382.

Fujita Y., Ferris F. G., Lawson D. L., Colwell F. S., and Smith R. W. (2000) Calcium carbonate precipitation by ureolytic subsurface bacteria. *Geomicrobiol. J.* **17,** 305–318.

Hammes F., Seka A., de Kniff S., and Verstraete W. (2003) A novel approach to calcium removal from calcium-rich industrial wastewater. *Water Res.* **37,** 699–704.

Helgeson H. C. (1969) Thermodynamics of hydrothermal systems at elevated temperatures and pressures. *Am. J. Sci.* **267,** 729–804.

Kepner R. L. and Pratt J. R. (1994) Use of fluorochromes for direct enumeration of total bacteria in environmental-samples—Past and present. *Microbiol. Rev.* **58,** 603–615.

Knobel L. L., Bartholomay R. C., Cecil L. D., Tucker B. J., and Wegner S. J. (1992) Chemical Constituents in the Dissolved and Suspended Fractions of Ground Water from Selected Sites, Idaho National Engineering Laboratory and Vicinity, 1989. U.S. Geological Survey, Idaho.

Knorst M. T., Neubert R., and Wohlrab W. (1997) Analytical methods for measuring urea in pharmaceutical formulations. *J. Pharm. Biomed. Anal.* **15,** 1627–1632.

Lebron I. and Suarez D. L. (1996) Calcite nucleation and precipitation kinetics as affected by dissolved organic matter at 25 °C and pH >7.5. *Geochim. Cosmochim. Acta* **60,** 2765–2776.

Lorens R. B. (1981) Sr, Cd, Mn and Co distribution coefficients in calcite as a function of calcite precipitation rate. *Geochim. Cosmochim. Acta* **45,** 553–561.

McGenity T. J. and Sellwood B. W. (1999) New approaches to studying the microbial precipitation of carbonate minerals. *Sediment. Geol.* **126 (***1–4***),** 5–8.

Mobley H. L. and Hausinger R. P. (1989) Microbial ureases: Significance, regulation, and molecular characterization. *Microbiol Rev.* **53,** 85–108.

Mucci A. and Morse J. W. (1983) The incorporation of Mg^{2+} and Sr^{2+} into calcite overgrowths—Influences of growth-rate and solution composition. *Geochim. Cosmochim. Acta* **47,** 217–233.

Parkman R. H., Charnock J. M., Livens F. R., and Vaughan D. J. (1998) A study of the interaction of strontium ions in aqueous solution with the surfaces of calcite and kaolinite. *Geochim. Cosmochim. Acta* **62,** 1481–1492.

Pingitore N. E. and Eastman M. P. (1986) The coprecipitation of Sr^{2+} with calcite at 25 °C and 1 atm. *Geochim. Cosmochim. Acta* **50,** 2195–2203.

Pingitore N. E., Lytle F. W., Davies B. M., Eastman M. P., Eller P. G., and Larson E. M. (1992) Mode of incorporation of Sr^{2+} in calcite—Determination by X-ray absorption-spectroscopy. *Geochim. Cosmochim. Acta* **56,** 1531–1538.

Prieto M., Fernandez Gonzalez A., Putnis A., and Fernandez Diaz L. (1997) Nucleation, growth, and zoning phenomena in crystallizing $(Ba,Sr)CO_3$, $Ba(SO_4,CrO_4)$, $(Ba,Sr)SO_4$, and $(Cd,Ca)CO_3$ solid solutions from aqueous solutions. *Geochim. Cosmochim. Acta* **61,** 3383–3397.

Ramachandran S. K., Ramakrishnan V., and Bang S. S. (2001) Remediation of concrete using micro-organisms. *ACI Mater. J.* **98,** 3–9.

Reeder R. J., Lamble G. M., and Northrup P. A. (1999) XAFS study of the coordination and local relaxation around Co^{2+}, Zn^{2+}, Pb^{2+}, and Ba^{2+} trace elements. *Am. Miner.* **84 (***7–8***),** 1049–1060.

Riley R. G. and Zachara J. M. (1992) *Chemical Contaminants on DOE Lands and Selection of Contaminant Mixtures for Subsurface Science Research.* U.S. Department of Energy, Office of Energy Research.

Rimstidt J. D., Balog A., and Webb J. (1998) Distribution of trace elements between carbonate minerals and aqueous solutions. *Geochim. Cosmochim. Acta* **62,** 1851–1863.

Roden E. E., Leonardo M. R., and Ferris F. G. (2002) Immobilization of strontium during iron biomineralization coupled to dissimilatory hydrous ferric oxide reduction. *Geochim. Cosmochim. Acta* **66,** 2823–2839.

Schueler B., Sander P., and Reed D. A. (1990) A time-of-flight secondary ion microscope. *Vacuum* **41 (***7–9***),** 1661–1664.

Schultzelam S. and Beveridge T. J. (1994) Nucleation of celestite and strontianite on a cyanobacterial S-layer. *Appl. Environ. Microbiol.* **60,** 447–453.

Stocks-Fischer S., Galinat J. K., and Bang S. S. (1999) Microbiological precipitation of $CaCO_3$. *Soil Biol. Biochem.* **31,** 1563–1571.

Teng H. H., Dove P. M., and De Yoreo J. J. (2000) Kinetics of calcite growth: Surface processes and relationships to macroscopic rate laws. *Geochim. Cosmochim. Acta* **64,** 2255–2266.

Tesoriero A. J. and Pankow J. F. (1996) Solid solution partitioning of Sr^{2+}, Ba^{2+}, and Cd^{2+} to calcite. *Geochim. Cosmochim. Acta* **60,** 1053–1063.

Tobin K. J., Colwell F. S., Onstott T. C., and Smith R. (2000) Recent calcite spar in an aquifer waste plume: A possible example of contamination driven calcite precipitation. *Chem. Geol.* **169 (***3–4***),** 449–460.

Warren L. A., Maurice P. A., Parmar N., and Ferris F. G. (2001) Microbially mediated calcium carbonate precipitation: Implications for interpreting calcite precipitation and for solid-phase capture of inorganic contaminants. *Geomicrobiol. J.* **18,** 93–115.

Wiedemeier T. H., Rifai H. S., Newell C. J. and Wilson J. T. (1999) *Natural Attenuation of Fuels and Chlorinated Solvents.* Wiley.

Wood W. W. and Low W. H. (1986) Aqueous geochemistry and diagenesis in the Eastern Snake River plain aquifer system, Idaho. *Geol. Soc. Am. Bull.* **97,** 1456–1466.